Construction and Building Materials 360 (2022) 129527

Contents lists available at ScienceDirect

Construction and Building Materials

journal homepage: www.elsevier.com/locate/conbuildmat

Influence of limestone addition on sodium sulphate activated blast furnace slag cements

Alastair T.M. Marsh, Zengliang Yue, Yuvaraj Dhandapani, Katharine Button, Samuel Adu-Amankwah, Susan A. Bernal *

School of Civil Engineering, University of Leeds, Leeds LS2 9JT, United Kingdom

ARTICLE INFO

Keywords:
Blast furnace slag
Limestone
Alkali-activated cements
Hybrid cements
Reaction kinetics
C-A-S-H
Ettringite

ABSTRACT

The effect of limestone replacement in the reaction and phase assemblage evolution of two sodium sulfate activated slag cements was investigated. The slag composition and its reactivity influenced the reaction kinetics of these materials. Paste with limestone addition exhibited an acceleration in reaction kinetics, particularly for slowly reacting slags. Ettringite and an aluminium substituted calcium silicate hydrate were identified as main reaction products in these cements, independently of the slag type or limestone replacement level. No significant changes in phase assemblages were observed with limestone addition for over 365 days of testing; however, these composite cements exhibited an increased compressive strength, consistent with a refined pore structure. These results indicate that it is possible to partially replace slag by limestone in sulfate activated slag cements without changing the type of reaction products forming in these systems, while also increasing compressive strength and achieving a similar refined pore structure.

1. Introduction

Reducing the Portland clinker content in cements for the production of concrete, is one of the most viable and well accepted strategies to reduce the environmental impact associated with the construction sector [1]. The use of high volumes of supplementary cementitious materials (SCMs) is strongly dependent on their chemical reactivity, and the performance developed by the concretes produced with them [2]. In order to optimise reaction kinetics and enhance strength development in systems with high SCMs content (>70 %), the addition of alkaline substances has been investigated. The rationale for these additions is the ability of alkaline substances to accelerate ordinary Portland cement (OPC) hydration [3]. Composite cementitious systems comprising OPC, a SCM and an alkaline substance are referred to as hybrid alkaline cements [4]. These mixtures take advantage of the hydration mechanism of OPC, combined with the reaction mechanism taking place during alkali-activation of aluminosilicate precursors. This produces binders with desirable properties, and reduced global warming potential [5].

Hybrid alkaline cements have been extensively studied over the past decades. The focus has been on systems based on pulverized fly ashes and Portland cement/clinker, mainly using sodium hydroxide or sodium silicate type activators [6–8]. Given the great potential for producing concretes with very low Portland cement contents when using these binders, a significant number of studies have been published in this topic over the past decade [4,9–11]. These studies discussed the reaction mechanism of these materials, the factors which control their phase assemblages and strength development, and also the research needs for determination of their durability performance. From this literature, it is known that the features of these systems are controlled by several factors. These include: the chemical composition, physical and mineralogical properties of the precursors used; activator type and dose; and, curing conditions. These factors consequently control their mechanical and transport properties. More recent studies have focused on assessing the performance of hybrid alkaline cements produced with milder activators, such as sodium sulfate [12–17]. Understanding hybrid sodium sulfate cement systems requires evaluation of the potential interaction of each of their components with this activator.

The effect of sodium sulfate addition on OPC hydration has been extensively studied, particularly the potential formation of the so-called U-phase ($4CaO{\cdot}0.9Al_2O_3{\cdot}1.1SO_3{\cdot}0.5Na_2O{\cdot}16H_2O$) [18]. This phase is typically identified upon hydration of OPC under highly alkaline conditions, such as those achieved when adding high concentrations (10–15 wt%) of sodium sulfate [19]. The high alkalinity in those systems is achieved via the chemical reaction of sodium sulfate with portlandite

* Corresponding author.
E-mail address: s.a.bernallopez@leeds.ac.uk (S.A. Bernal).

https://doi.org/10.1016/j.conbuildmat.2022.129527
Received 15 July 2022; Received in revised form 26 September 2022; Accepted 18 October 2022
Available online 3 November 2022
0950-0618/© 2023 The Authors. Published by Elsevier Ltd. This is an open access article under the CC BY license (http://creativecommons.org/licenses/by/4.0/).

(as tricalcium aluminate hydration progresses), leading to the formation of sodium hydroxide and gypsum [20]. Secondary formation of the U-phase and other sulfate-bearing phases is linked to degradation of OPC-based concretes [21,22]. This is one of the reasons why the use of sodium sulfate in OPC systems has been very limited. Despite these potential risks, in recent years there has been a burgeoning interest in exploring the effects of alkalis in the hydration of clinker phases [23,24]. This is in order to identify optimised concentrations for their potential utilisation in cements produced with high volumes of SCMs.

On the other hand, the interactions between sodium sulfate and SCMs has been more widely studied within the context of alkali activation. Most studies of sodium sulfate activated slag cements have focused on evaluating the type of reaction products formed using a single source of slag precursor, or determining the strength development of such systems [25,26]. Very few studies have evaluated the phase assemblage evolutions of these cements. The main reaction product has been identified as an aluminium substituted calcium silicate hydrate (C-A-S-H), and as main secondary reaction product, ettringite has been reported [27,28]. Different properties such as slag fineness [29] and activator dose [30] have been evaluated in these systems – with increasing slag fineness and increasing activator dose, a higher degree of slag reaction is achieved. It has been demonstrated that different reaction products are obtained with slight changes in Al_2O_3 or MgO content in the slags activated with either hydroxide or silicate activators [31,32]. However, there is no understanding about the effect of slag chemistry on the phase assemblage of sodium sulfate activated systems. This is a knowledge gap to be evaluated in the present study.

To future-proof the development of low carbon binders such as hybrid sodium sulfate activated cement, lowering the slag fraction in these systems needs to be considered. This can be achieved by addition of limestone. Limestone is widely used in the construction sector and its effect is very well documented when producing binary and ternary cements [33] including its reaction mechanism [34]. The use of limestone has also been investigated in the production of ternary blended cements including slag [35] or calcined clays [36,37]. In ternary systems, it has been stated that the synergetic effect between limestone and SCMs offers significant advantages for production of sustainable cements. However, the investigation of the effects of limestone in hybrid alkaline cements has been very limited [38,39] and often restricted to the early curing ages (28 days of curing). Therefore, it remains largely unknown whether limestone will act as a filler or can potentially react in these systems, particularly in the longer term.

In response to these knowledge gaps, in this study two commercial blast furnace slags with different MgO/Al_2O_3 ratios were activated with sodium sulfate. The level of slag substitution by limestone was varied, and the effect on the phase assemblage evolution of cured pastes was evaluated for up to one year. Reaction kinetics were evaluated via isothermal calorimetry. Changes in phase assemblage were determined following a multi-technique approach applying X-ray diffraction, thermogravimetry coupled with mass spectrometry and solid state nuclear magnetic resonance spectroscopy. Compressive strength and pore structure were determined in specimens after 28 days of curing.

2. Experimental methodology

2.1. Materials

Oxide compositions of the two blast furnace slags and limestone used in this study were determined by X-ray fluorescence (XRF), using a fused bead preparation method in a Rigaku ZSX Primus II (Table 1). XRD patterns for the precursor slags are provided in the Supplementary Information.

The particle size distributions of the two slags and limestone were measured with a Malvern Mastersizer 2000 laser diffractometer, using isopropanol as the dispersion liquid. The particle size distribution of the two anhydrous slags were comparable with an average d_{50} of 11.7 μm for slag 1 (S1) and 12.5 μm for slag 2 (S2). The limestone used in this study was slightly coarser than the slags, with a d_{50} of 15.3 μm. The full particle size distribution curves for the precursor materials are provided in the Supplementary Information where no significant differences are identified between the two slags studied.

2.2. Mix design and sample preparation

The mix design of the evaluated pastes is presented in Table 2. As activator an anhydrous sodium sulfate powder (Acros Organics, Na_2SO_4 > 99 %) was used, which was dissolved in deionized water at 40 °C and cooled down to room temperature (20 °C) prior to use. The sodium sulfate-activated slags with replacements of 5 wt.% and 10 wt.% limestone (relative to mass of slag) were prepared with an activator dose of 8 g Na_2SO_4 per 100 g anhydrous precursors (slag + limestone) and a water to solids (slag + limestone + sodium sulfate) ratio of 0.4. To generate homogeneous mixtures of the anhydrous precursors, a roller ball mill (Capco Ball Mill Jar 2VS) was used to blend the slag and limestone using soft plastic balls for 3 h.

The solid precursors (i.e. slag or slag + limestone powders) were then mixed with the activating solution by hand for 3 min to obtain a uniform cementitious paste. The produced paste was cast in 5 mL centrifuge tubes, and then sealed and stored in a water bath at 21 °C until testing.

2.3. Testing methods

2.3.1. Kinetics of reaction

In fresh pastes, isothermal calorimetry experiments were conducted using a TAM Air Calorimeter at 20 ± 0.02 °C. The fresh pastes were prepared by hand-mixing for 3 min. 9 g of paste was weighed into an

Table 2
Mix design of sulfate activated slag/ limestone blended cements.

Sample ID	Slag (g)	Limestone (g)	Anhydrous Na_2SO_4 (g)	w/s*
100S1	100	0	8	0.4
95S1	95	5	8	0.4
90S1	90	10	8	0.4
100S2	100	0	8	0.4
95S2	95	5	8	0.4
90S2	90	10	8	0.4

* w/s – stands for water/solids ratio.

Table 1
Chemical oxide compositions of the anhydrous slags and limestone.

Precursors	Oxides (wt.%)										
	CaO	SiO_2	Al_2O_3	MgO	SO_3	Fe_2O_3	TiO_2	MnO	K_2O	Others	LOI*
Slag 1 (S1)	43.6	33.6	11.3	5.4	3.3	0.5	1.1	0.3	0.5	0.4	–
Slag 2 (S2)	44.4	35.7	9.8	6.3	1.6	0.4	0.6	0.3	0.4	0.5	0.1
Limestone (LS)	53.9	2.2	0.9	0.7	0.2	0.2	–	–	0.1	–	41.4

*Loss on ignition (LOI) determined at 900 °C.

ampoule and immediately placed in the calorimeter to record heat flow up to 15 days. Reference samples containing quartz and distilled water (9 g in total) were used, and all heat flow and cumulative heat measurements were normalized by the total mass of paste.

2.3.2. Phase assemblage characterisation

After 7, 28, 180 and 365 days of curing, specimens were ground and immediately characterised without any solvent exchange treatment to arrest reaction. Hydration stopping was not performed in order to minimise modifications to hydrated phases. This precaution was carried out with ettringite in mind - ettringite was expected to be formed in these systems, and its sensitivity upon solvent exchange treatment is well known [40,41]. Microstructural characterisation of these samples was conducted via:

- X-ray diffraction (XRD), using a PANanalytical MPD Pro with Cu-Kα radiation and a nickel filter. A 10 mm incident beam mask was used with automatic incident divergence and fixed anti-scatter slits. The tests were conducted with a step size of 0.03° and a counting time of 1 s/step, from 5° to 70° 2θ. X'pert Highscore plus V5.1 was used for phase identification using PDF-4 + 2022 ICDD database. Additionally, search by composition was carried using PDF 4 + database software to identify some of the phases formed at a longer curing period.
- Thermogravimetric analysis coupled with mass spectrometry (TG-MS), using a Netzsch STA 449 F5 coupled with a Netzsch QMS 403D mass spectrometry unit. In each case, 30 mg of sample was tested from 35 to 1000 °C at a heating rate of 10 °C/min under nitrogen flowing at 60 mL/min. A 10 minute isotherm at 30 °C under nitrogen flow was performed before starting the heating ramp.

To quantify the calcite content in the pastes over different curing durations, the mass loss identified between 600 and 800 °C was determined (WL_{CaCO3}). The percentage of reacted $CaCO_3$ (relative to the mass of solid pastes) was then calculated considering the molecular masses of $CaCO_3$ (M_{CaCO3} = 100 g/mol) and CO_2 (M_{CO2} = 44 g/mol) via the equation below:

$$Wt_{reacted\ CaCO_3} = WLi - WL_{CaCO_3} \times \frac{M_{CaCO_3}}{M_{CO_2}} \quad (1)$$

Where the *WLi* represents the amount of limestone in the system.

- Solid-state magic angle spinning (MAS) nuclear magnetic resonance (NMR) spectra were collected using a Bruker Avance III HD spectrometer with a 400 MHz wide bore magnet (magnetic field 9.4 T). ^{29}Si MAS NMR spectra were collected at an operating frequency of 79.5 MHz, using a zirconia rotor and spun at 6 kHz in a 7 mm solid-state MAS probe, and employed a 90° pulse of duration 5.5 μs, a relaxation delay of 40 s and a minimum of 2,048 scans. Solid-state ^{27}Al MAS NMR spectra were collected at an operating frequency of 104.3 MHz, using a zirconia rotor and spun at 12 kHz in a 2.5 mm solid-state MAS probe, and employed a 90° pulse of duration 0.23 μs, a relaxation delay of 0.5 s and a minimum of 8,192 scans. ^{29}Si and ^{27}Al chemical shifts were referenced to external samples of tetramethylsilane (TMS), and Yttrium Aluminium Garnet (YAG) respectively, the latter with the *hexa*-coordinated site referenced to 0.7 ppm. Signals were normalized by area under the curve before plotting [42].

2.3.3. Compressive strength and porosity testing

After 28 days of sealed curing, paste cubes of 25 mm × 25 mm were used for testing compressive strength with loading speed of 2.4 kN/s using an Instron 3382.

The pore size distributions of the paste specimens were determined via Mercury intrusion porosimetry (MIP), using MicroActive AutoPore V9600 Version 1.02. Cylindrical specimens of 1 cm diameter and 1 cm length were quartered and then prepared for MIP measurements. Prior to the test, the specimens were immersed in isopropanol for 48 h. The solution was changed after 6 and 24 h. The samples were then placed in a vacuum desiccator for 1 week. About 0.86 g of sample was run with a head size of 5 cc and stem volume of 1.131, and intruded with mercury at a rate of 0.1–61,000 psi at 22 °C. The intrusion data was then converted into equivalent pore entry diameter size, taking the contact angle to be 130°.

Unfortunately compressive strength and MIP tests at other curing durations could not be conducted due to laboratory access restrictions during the COVID-19 pandemic.

3. Results and discussion

3.1. Reaction kinetics

Fig. 1 presents the heat flow and cumulative heat for the two slag pastes in the presence of sodium sulfate solution, as a function of the limestone content. Significant differences in the kinetics of reaction were observed as a function of the slag composition. For the S1 series (Fig. 1.A) a sharp and high intensity heat flow peak, associated with the acceleration/deceleration period, was observed independently of the addition of different amounts of limestone. Maximum heat flow occurred at 23 h of reaction. Conversely for the S2 series (Fig. 1B), a pre-induction period was observed soon after placing the pastes in the calorimeter, followed by a dormant period from 10 h up to 100 h. This dormant period was shorter for the paste containing 10 wt% limestone (90S2). The acceleration/deceleration curves presented a similar shape, independent of the addition of limestone. The asymmetry of the curve associated with the deceleration period was more pronounced for the S2 series, compared with S1. This indicates that precipitation of reaction products in the S2 slag cements continued taking place for a longer duration. The majority of calorimetry results of sodium sulfate activated slag cements reported in other studies [29,30] are comparable to those obtained for the S1 series, where an induction/dormant period has not been previously identified.

Considering the effect of the limestone additions - the cumulative heat curves for the S1 slag series (Fig. 1C) showed that 400 h after mixing, the slag activated without limestone addition (100S1) exhibited a lower cumulative heat than the pastes containing limestone additions (95S1 and 90S1). This indicated a lower extent of reaction products formation in the 100S1 paste, compared to the 95S1 and 90S1 pastes. Negligible differences were observed between samples with 5 wt.% (95S1) and 10 wt.% (90S1) limestone addition. In contrast, for the S2 slag series, clear differences in the kinetics of reaction were identified between the paste samples with 5 wt.% (95S2) and 10 wt.% (90S2) addition of limestone.

The presence of limestone is known to act as nucleation sites for reaction products [37], which accelerates reaction kinetics; and, to increase Ca^{2+} concentration [43], which enhances the formation of reaction products. But to help interpret the apparent difference in effects of limestone additions on the reaction kinetics of the slag S1 and slag S2 samples, it is crucial to note that the slag S2-based samples had a significantly longer induction period. It is likely that the longer induction period in the slag S2 samples (relative to the slag S1 samples) facilitated acceleration due to limestone, specifically with the 10 wt.% addition [37]. It is not obvious why the 5 wt.% addition had a seemingly negligible effect on reaction kinetics of slag 2, relative to the 10 wt.% addition. Nonetheless, on the basis of cumulative heat at 400 h, the slag S2 pastes with 5 wt.% and 10 wt.% limestone addition seemed to undergo a comparable extent of reaction. Hence, enhanced reaction kinetics is likely to be mainly due to filler action during the acceleration stage [44].

Considering the slag S1 series - the majority of the slag reaction occurred within the first 24 h, and hence masked any acceleration due to

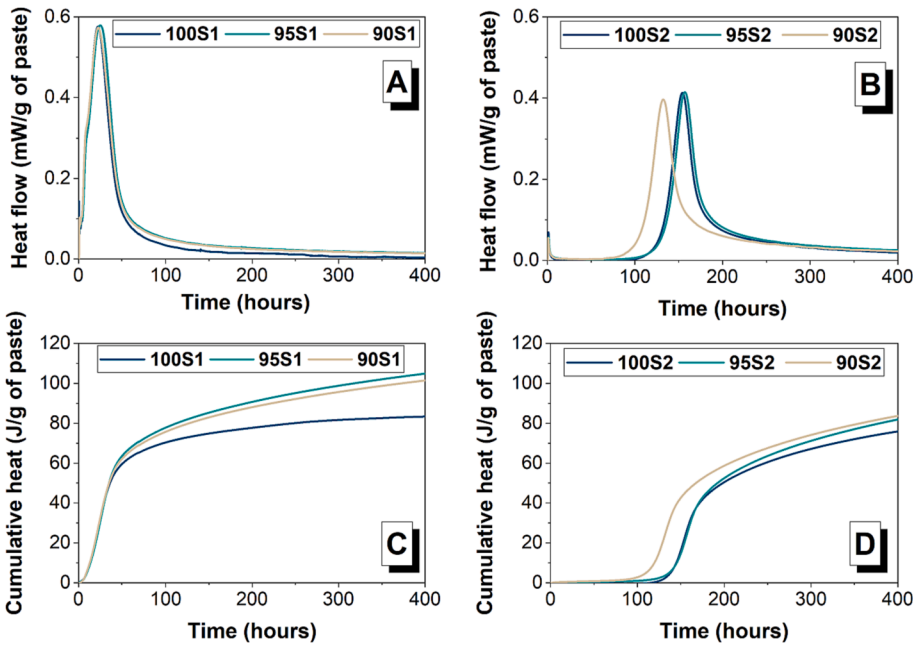

Fig. 1. Isothermal calorimetry results of Na_2SO_4-activated slag as a function of limestone content. Heat flow and cumulative heat curves correspond to S1 (A, C) and S2 (B,D) respectively.

the limestone addition. However, the enhancement in heat release with limestone addition is noticeable beyond 24 h. For the S2 series, the differences in cumulative heat between the paste solely based on slag and those containing limestone was modest, especially when compared with the results of the S1 series. In comparison, for the S1 series the cumulative heat was significantly lower in the absence of limestone. On the basis of cumulative heat, the degree of reaction of pastes produced with slag S2 was consistently lower than for the pastes produced with slag S1.

Comparing between the two precursor slags - the differences in heat release between the two slags suggest that the slag composition has a significant effect on the kinetics of reaction of sodium sulfate-activated slag systems. These results differ to previous studies on alkali-activated slag cements produced with sodium hydroxide or silicate activators, which reported that a higher Al_2O_3 content (7 wt.% to 16.7 wt.%) with a moderated content of MgO (6.4 wt% – 7.2 wt.%) led to lower degree of reaction [45]. This consequently led to the development of materials with higher porosity and reduced mechanical strength. When using hydroxide or silicate activors these observations have been attributed to the importance of the MgO/Al_2O_3 ratio in these materials. The subsequent influence on the formation and precipitation of Al-bearing secondary phases in these cements, particularly hydrotalcites, is believed to be significant.

The results for the sodium sulfate activated slag cements evaluated here are, however, in good agreement with what has been observed for sulpersulfated cements [46] whose main Al-bearing phase is ettringite, and, also similar to what has been reported for sodium sulfate activated slag cements [25]. In a recent study evaluating the chemical reactivity of commercial slags applying the *R*3 test method [47], slags with higher contents of Al_2O_3 seemed to be more reactive at early ages. This highlights that slag composition alone is not appropriate as a universal indicator for how a given slag might react, as this seems to be specific to the cementitious system that is being evaluated. The nature of the glassy phase is also a parameter of interest with regards to reactivity – this is explored in Section 3.2.3.

Independent of the slag composition, the addition of limestone accelerated the kinetics of reaction of the composite cements. This was more noticeable in the pastes produced with slag S2 during the first hours of reaction, and in the pastes produced with slag S1 after 50 h of the reaction. A similar effect of limestone addition has been reported for ternary OPC, slag, limestone composite cements [48] - it seems likely that a similar mechanism of enhancing the nucleation of gel phases is taking place in these systems [35].

3.2. Phase assemblage evolution

3.2.1. X- ray diffraction

Figs. 2 and 3 present the X-ray diffraction patterns of sodium sulfate activated composite cements produced with S1 and S2 respectively, as a function of curing time. The main crystalline reaction products identified in all the cements evaluated in this study are: ettringite (E) (powder diffraction file (PDF) #00-013-0350) and calcium silicate hydrate (tobermorite 9 Å, CSH, PDF# 00-010-0374) or an aluminium-substituted calcium silicate hydrate (Al-tobermorite, C-A-S-H, PDF# 00-019-0052). Independently of the slag composition, ettringite was identified at 7 days of curing, and it remained stable for up to 365 days without any noticeable conversion to monosulfate phase with curing time or limestone addition.

Calcite (CC, PDF #00-024-0027) was observed in the diffractograms of 90S1 (Fig. 2B) and 90S2 (Fig. 3B), consistent with the addition of limestone in these systems. The addition of limestone did not seem to contribute to the formation of new crystalline reaction products, indendepently of the slag composition or curing time.

In the pastes solely based on slag, the reflections attributed to ettringite were more intense in pastes produced with slag S1 (Fig. 2A) compared to those produced with slag S2 (Fig. 3A). This could be attributed to the higher alumina content in slag S1 (Table 1). Similar results have also been obtained in super sulphated slag cement, with more ettringite formation observed when using slags with higher Al content [46]. Slag S1 also had a higher sulphur content compared to Slag 2, as determined from XRF (Table 1). A higher sulphur content might be expected to contribute to more ettringite formation. However, an XRF measurement does not distinguish sulphur speciation, or the phases in which sulphur is present. Therefore, it is not possible to make a causal link between the higher sulphur content in Slag S1, and the higher ettringite formation in the pastes produced with Slag S1. Calcium silicate hydrate (C-S-H) and/or calcium aluminate silicate hydrate (C-A-S-H) with a tobermorite type structure, were identified as the other major

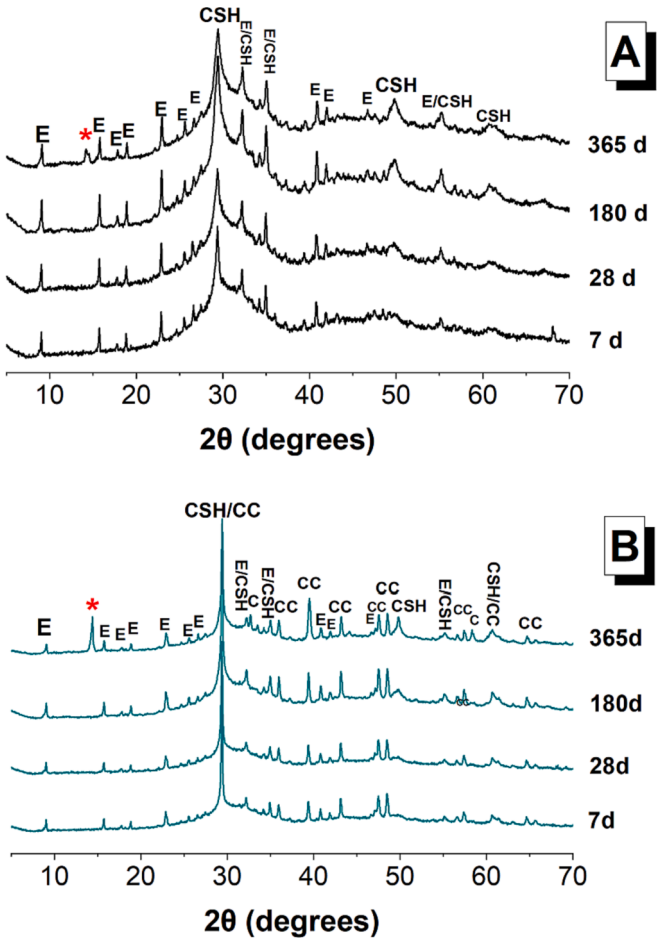
A
CSH
E/CSH
E/CSH
E
E
E

Formation of zeolite type phases in alkali-activated slag cements is rare and unexpected for the cements evaluated in this study. Formation of gismondine and garronite (both GIS framework type) zeolite phases was reported in silicate activated slag/metakaolin cements, produced with a slag with very low (<2 wt%) MgO content [54–56]. Thermodynamic modelling simulations for sodium sulfate activated slag cements [57] do not predict formation of these phases, despite zeolite phases being included in the database when simulations were performed. However, it is acknowledged that the stability of zeolitic phases and their transformation from semi-crystalline precursors are very sensitive to both thermodynamic and kinetic parameters [58,59] and so their formation cannot be conclusively discounted on the basis of thermodynamic modelling.

Jackson et al. [60] analyzed the structure of C-(A)-S-H type phases forming in ancient Roman cements exposed to seawater, which is well known to be a sulfate rich environment. It was identified in those specimens that C-(A)-S-H phases presented a highly crosslinked Al-Tobermorite type structure with reflections at a similar position to that of the unidentified peak in this study. Considering alkali aluminosilicate systems in the broadest sense, there is a thermodynamic driving force for metastable phases to transform to more highly ordered phases over time [58,59]. Hence, it could be hypothesized that the unidentified peak could be indicating structural changes (ordering) in the C-(A)-S-H type phases forming in sodium sulfate activated slag systems over extended curing durations.

3.2.2. ^{29}Si MAS NMR spectroscopy

Solid state NMR has particular value for distinguishing the presence of atoms and their structural configurations in crystalline phases. It also provides unique information about the structure of poorly crystalline phases, which may not easily be detectable by using XRD. Conventional Qn(NAl) notation is used for Si bonding environments, whereby n refers to the number of -O-Si 'bridges' to nearest neighbour sites, and N refers to the number of Al next-nearest-neighbour sites [61].

The unreacted slags exhibited very similar ^{29}Si MAS NMR spectra (Fig. 4) with a resonance centred at $\delta i_{so} = -74$ ppm, in line with blast furnace slags' highly disordered, melilite-like structure as described elsewhere [62]. It is worth mentioning that deconvolution of the spectra was not carried out in this study. The method assumes that the anhydrous slag is dissolved congruently, which is generally true in highly alkaline conditions, such as those achieved in NaOH and Na_2SiO_3-activated slag systems [32,63]. The congruent dissolution of glassy calcium aluminosilicate requires the pH of the activator to be over 12.5 [64]. In contrast, the initial pH value of the Na_2SO_4 solution used in this study was almost 7. Although the pH of the solution was expected to increase as the reaction progressed, it would not be appropriate to assume that the slag dissolved congruently under these conditions.

For sodium sulfate-activated slag cements without limestone addition (100S1 and 100S2) the ^{29}Si MAS NMR spectra (Fig. 4) exhibited three resonances centred at $\delta i_{so} = -79$ ppm, -82 ppm and -85 ppm, attributed to Q^1, Q^2(1Al) and Q^2 sites, respectively. These resonances are predominantly attributed to C-(A)-S-H gel typically identified in alkali-activated slag cements [65]. This is the only Si-bearing product phase identified in the sodium sulfate activated systems when analysed by XRD (Fig. 2 and Fig. 3). Some extent of Na^+ uptake is expected into the gel phase, both in interlayer sites and sorbed to gel surface sites [66,67] therefore these type of gels can be described more accurately as C-(N)-A-S-H. However, there is likely some overlap in this Q^1 and Q^2 region with unreacted slag. The shoulder downfield of Q^1(II) is associated with Q^0 and Q^1(I) sites [68]. In sodium metasilicate activated slag systems, the broad resonance upfield of Q^2 sites at $\delta i_{so} > 90$ ppm has been assigned to Q^4 sites in sodium aluminosilicate hydrate (*N*-A-S-H) type gels, or/and the Q^3 site in C-(A)-S-H gel [65]. In the cements assessed in this study such resonances are not clearly identifiable, consistent with ^{29}Si MAS NMR results of sodium sulfate activated slag cements reported elsewhere [28,30].

In all the cements evaluated, a decrease in intensity of the broad shoulder in the $\delta i_{so} = -70$ to -78 ppm region was observed in the spectra for 180 days curing time compared to 28 days, along with an increase in the intensity of the Q^2 sites. This indicates that further reaction of slag occurred over this time period [63], consistent with the observation by XRD (Figs. 2 and 3). This effect was slightly more pronounced for the slag S1 systems compared to the S2 systems, consistent with the calorimetry results (Fig. 1) which indicated a reduced reactivity of S2 under the activation conditions assessed in this study. This further reaction of slag over extended curing periods results in additional formation of C-(A)-S-H in these systems [30]. However, given the constraints on deconvolution, this cannot be quantified. On the other hand, the higher intensity of Q^1(II) in S1 indicates higher chain-end sites balanced by Ca^{2+} or Al^V ions [68]. The higher intensity of Q^2 sites in S2 suggests a higher mean chain length.

In terms of the influence of limestone addition, the decreased intensity in the shoulder between $\delta i_{so} = -70$ and -78 ppm was more pronounced in the systems with limestone substitution. This indicates that a higher degree of slag reaction was achieved with the addition of limestone. The higher intensity in Q^2 and Q^3 sites in 90S1 and 90S2 after 180 days suggests that the addition of limestone increased the connectivity of C-(N)-A-S-H type gel.

These results demonstrate that the structure of the C-(A)-S-H type gels forming in the two sodium sulfate activated slag cement systems evaluated is comparable - the addition of limestone is not inducing significant structural changes in this reaction product. Even accounting for the possibility that zeolitic phases that form in cementitious systems can be disordered [69], there is no evidence of formation of highly crosslinked Q^4 ($\delta_{iso} > 90$ ppm) sites typically present in zeolites [70], at least up to 180 days of curing.

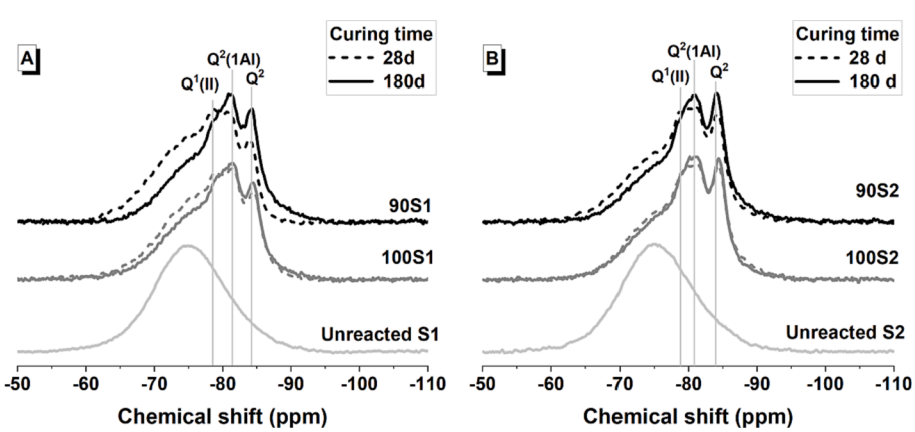

Fig. 4. ^{29}Si MAS NMR spectra of slag precursors and sodium sulfate activated slag pastes as a function of slag type (A) S1 and (B) S2, and curing duration.

3.2.3. ^{27}Al MAS NMR spectroscopy

^{27}Al MAS NMR spectra were collected for all specimens for up to 365 days and results are presented in Fig. 5 and Fig. 6, for slag S1 and slag S2, respectively. $q^n(X)$ notation is used to describe Al bonding environments – this is analogous to $Q^n(NAl)$ notation for Si environments, whereby n refers to the number of -O-Si 'bridges' to nearest neighbour sites, and N refers to the number of Al next-nearest-neighbour sites [71]. The spectra of the unreacted slags exhibited an asymmetric and broad resonance centred at δi_{so} = 58–59 ppm associated with Al^{IV} sites, consistent with the highly disordered nature of blast furnace slags [62].

Firstly, regarding the slag precursors themselves - it is helpful to consider the influence of any differences in the precursor slags' local chemical environments, when attempting to explain differences in their reaction kinetics and overall reactivity. In Section 3.1, the higher Al_2O_3 content of slag S1 was suggested as a potential cause of its faster reaction kinetics and higher overall reactivity. In addition to the overall content of Al in slag, the local chemical environments of Al is also consequential. When $[Al_2O_3/M_2O] < 1$ in an alkali aluminosilicate glass, the addition of Al^{3+} acts as a network former and causes the conversion of non-bridging oxygen (NBO) to bridging oxygen (BO) sites [72 73]. The reactivity of glassy phases is influenced by their extent of depolymerisation, which can in turn be described by the number of non-bridging oxygens per tetrahedrally coordinated cation [74].

Fig. 5 shows the ^{27}Al MAS NMR spectra of S1 and S2 precursor slags. The spectrum of slag S1 is slightly shifted to the right (relative to slag S2) in the region between 50 and 20 ppm, which corresponds to a higher amount of Al^V [75]. It should be noted that this shift is not related to the tail of the Al^{VI} peak between 20 and 0 ppm, as the spectra S1 and S2 overlay this region [75]. The second order quadrupolar interaction of the ^{27}Al MAS NMR ($S > 5/2$) causes broadening of peaks and hence an overlap [61,75]. The presence of the slight shift may represent a more significant change in reality.

It is plausible that the higher Al^V content in slag S1 partly explains the higher observed reactivity of slag S2. For slags with comparable CaO content to those used in this study, Wang et al. [76] reported that increased Al_2O_3 content only had a negative effect on reactivity when the Al_2O_3 content of slag exceeded 15 wt.%. However, given it is difficult to precisely identify the difference in Al^V content between the two slags, it is inconclusive how much of the difference in reactivity is attributable to the quantity of coordination of Al, relative to other factors (such as CaO and MgO content).

Considering the cured cement pastes - in the Al^{VI} region (between δ_{iso} = 20 to 50 ppm [77]) of all spectra, three distinctive resonances were identified. The resonance centred at δ_{iso} = 13 ppm is attributed to ettringite [78]. This resonance was sharp and intense in the slag S1 series (Fig. 5) at all the curing ages, consistent with the XRD results (Fig. 2). A low intensity shoulder centred at δ_{iso}= ~ 9 ppm was observed in these samples which cannot be attributed to a single phase. A resonance at this chemical shift is often attributed to layered double hydroxides (LDH). This could be either a Ca-Al LDH with a hydrocalumite-like structure, also referred to as AFm phases, such as monocarbo- or monosulfo- aluminates [78,79]; or Mg-Al LDHs such as hydrotalcite [80], typically identified as a secondary reaction product in silicate-activated slag cements [68,81]. XRD results (Fig. 2) did not indicate formation of crystalline carbonate-hydrotalcite in sodium sulfate activated slag cements. The crystallinity of LDH is strongly dependent on the cation in the interlayer, and it has been reported that the crystallinity of sulfate-LDHs is particularly low [80]. Considering the high concentration of sulfates in the cements evaluated in this study, it is plausible that poorly crystalline sulfate-LDHs might have formed.

A third resonance was also identified at δ_{iso} ~ 4 ppm, which in hydrated cements is often attributed to the third aluminate hydrate (TAH) [82]. This phase was thought to be an amorphous nanoscale aluminate hydrate phase precipitated at the surface of the C-(N)-A-S-H type gels. However, it has been demonstrated by Mohamed et al. [83] that this resonance is most likely silicate-bridging $[AlO_2(OH)_4]_5^-$ sites in C-A-S-H type gels and therefore the TAH does not exist. Negligible changes in the intensity of these sites were identified at different curing times in sodium sulfate activated cements.

In slag S1 activated cements, the addition of limestone (Fig. 5B, 90S1) led to the development of less intense ettringite resonances, compared with specimens without limestone (100S1). This observation was consistent with the XRD results (Fig. 3B). The resonances attributed to LDH and $[AlO_2(OH)_4]_5^-$ sites are identifiable in these spectra; however, no significant changes in intensities were observed at extended curing durations, or when compared with cements produced in the absence of limestone.

In the slag S2 activated cements' spectra (Fig. 6A) the resonances attributed to ettringite, LDHs and $[AlO_2(OH)_4]_5^-$ sites in the C-A-S-H type gels were better resolved compared with those in the spectra of the slag S1 based cements. In this case a lower intensity of the resonance assigned to ettringite was identified, compared with the results of the S1

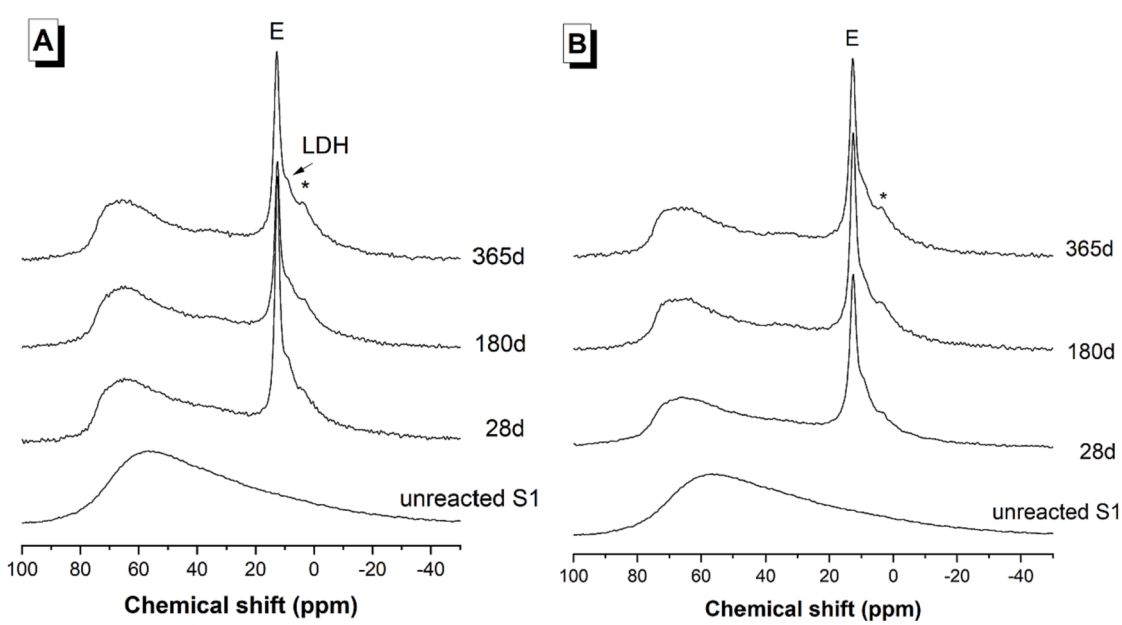

Fig. 5. ^{27}Al MAS NMR of sodium sulfate activated slag cements produced with slag S1 (A) without limestone addition and (B) with 10 wt.% limestone addition.

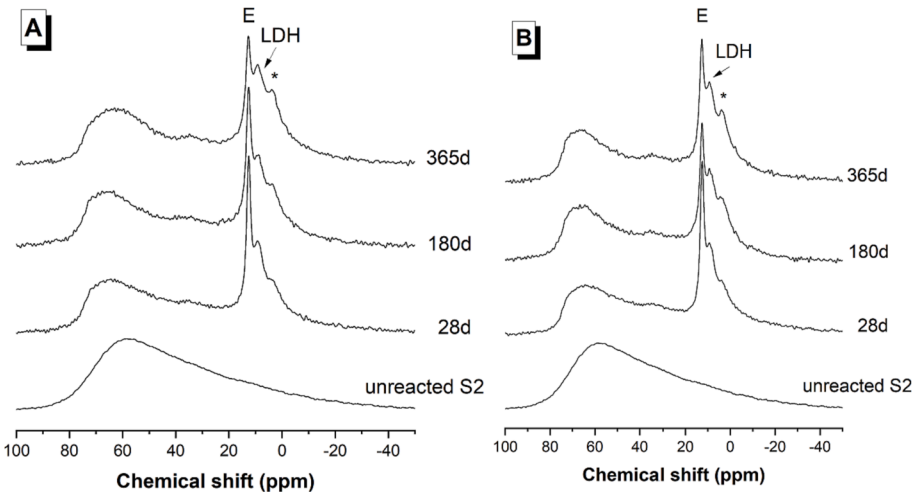

Fig. 6. ^{27}Al MAS NMR of sodium sulfate activated slag cements produced with slag S2 (A) without limestone addition and (B) with 10 wt.% limestone addition.

slag cements. This observation was consistent with the XRD results (Fig. 3). The intensity of the reflection centred at $\delta_{iso} \sim 9$ ppm seemed to increase at longer curing durations. This is an indicator that secondary reaction products, either Ca-Al or Mg-Al LDH, were continuously forming as the reaction progressed. It is hypothesised that the slightly higher MgO content of slag S2 might lead to formation of Mg-Al LDHs [31], particularly at extended curing duration (e.g. 365 days); however, it is not possible to distinguish the composition of the LDHs from ^{27}Al MAS NMR alone. Slight increases in the intensities of the reflections attributed to $[AlO_2(OH)_4]_5^-$ sites were identified at the different curing ages, consistent with a higher degree of reaction of the slag, particularly after 365 days. This is in agreement with observations from ^{29}Si MAS NMR (Fig. 4B).

In the Al^{IV} region (between $\delta_{iso} = 90$ to 40 ppm) an asymmetric and broad resonance was identified (Figs. 5 and 6) independently of the slag used or curing duration. This partly corresponds to the remnant unreacted slag present in the cement, and partly to the C-(N)-A-S-H type gels forming upon activation [63,68]. Whilst the spectrum in this region cannot be distinguished into its constituent peaks, the contributions to the measured spectrum from C-A-S-H type gels are anticipated to arise from q^2(I), q^2(II) [65] and q^3 [28] sites. The q^2(I) (73 ppm) and q^2(II) (67 ppm) sites are bridging tetrahedral sites, coordinated with different cationic interlayer species [65]. The q^3 coordinated aluminium (62 ppm) site is associated with a high degree of crosslinking in the C-A-S-H type gel [28]. Distinctive resonances attributable to q^4 Al in a zeolitic framework (associated with a peak in the range of ~ 50–65 ppm) [84,85] ^{27}Al MAS NMR spectra after 365 days of curing, were not observed.

No significant differences in either the shape or the intensity of the resonances in this region of the spectra were observed, independent of the curing age or addition of limestone (Figs. 5 and 6). It is known that increasing Ca:Si molar ratio in C-A-S-H leads to a preferred coordination state of Al^{VI} in cross-linking sites [86]. Given the Ca:Si molar ratio in both slags is an intermediate value (~1.4), one would expect an approximately equal distribution of Al between Al^{IV} and Al^{VI} cross-linking sites (excluding Al in secondary phases) [86].

Overall, limestone addition seems to have a negligible effect on the C-(N)-A-S-H structure, and on the relative quantities of LDH phases and ettringite forming in sodium sulfate activated slag cements.

3.2.4. Thermogravimetric analysis

Thermogravimetry curves for the sodium sulfate activated slag cements are presented in Fig. 7, and the total mass losses up to 1000 °C are reported in Table 3.

All cements exhibited (Table 3) a higher mass loss at longer curing

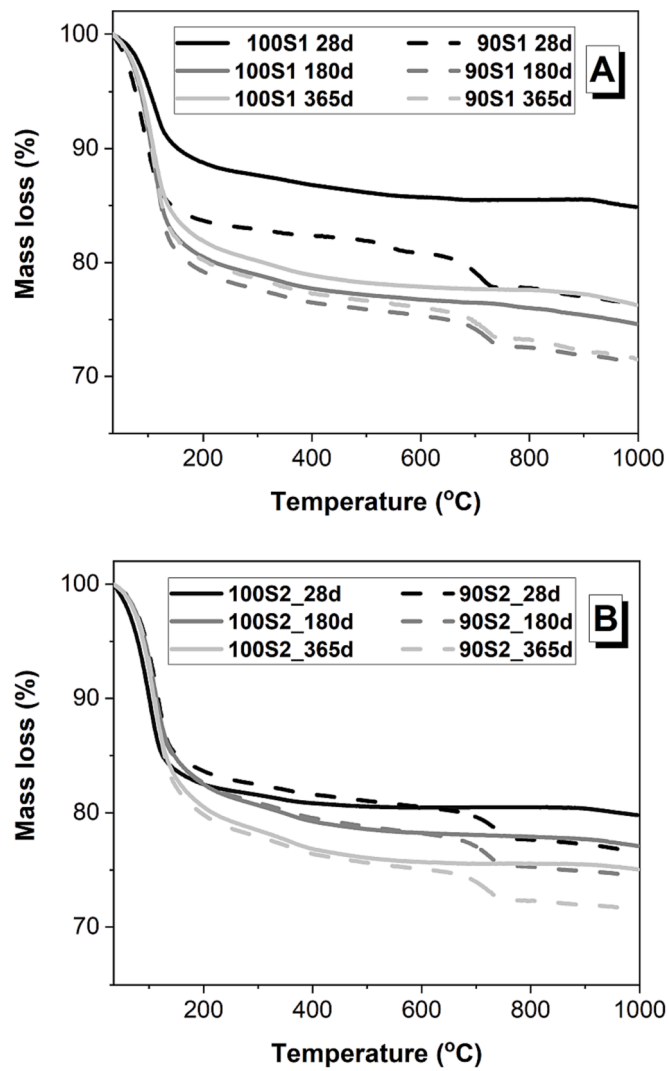

Fig. 7. Thermogravimetry curves of sodium sulfate activated slag cements produced with (A) slag S1 and (B) slag S2, as a function of limestone content and curing time.

Table 3
Total mass loss at 1000 °C determined by thermogravimetry of sodium sulfate-activated slag cements (±1%). LS = limestone.

Curing time (days)	S1		S2	
	0 wt% LS	10 wt% LS	0 wt% LS	10 wt% LS
28	15.1	23.8	20.2	23.6
180	23.8	28.8	22.9	25.7
365	25.5	28.8	25.1	28.5

durations, consistent with the decomposition of hydrated reaction products forming at higher degrees of slag reaction. A significant difference in the mass loss was observed between 100S1 and 100S2 at 28 days of curing. However, comparable total mass losses were identified for both slags after 180 and 365 days of curing, consistent with similar degrees of slag reaction in both of these cements.

Derivative curves along with mass spectrometry results for the S1 slag based cements are shown in Fig. 8. The mass loss below 200 °C is associated with dehydration of the C-A-S-H gel typically identified in this temperature range [87], and decomposition of ettringite which is typically observed at 114 °C [88]. These mass losses were greater at extended curing times, consistent with a higher degree of slag reaction as identified by XRD (Fig. 3) and ^{27}Al MAS NMR spectroscopy (Fig. 5). Mass losses between 400 °C and 800 °C are associated with decomposition of CO_2-bearing phases such as calcite [89]. In S1 slag samples without limestone (100S1) a low intensity mass loss peak was observed between 300 and 400 °C, accompanied by water release (Fig. 8B, 100S1). This might indicate the formation of traces of a Mg-Al LDH [90] in sodium sulfate activated slag cements. A mass loss between 700 °C and 1000 °C, accompanied by the release of SO_2 is likely linked to the unreacted slag fraction [91,92] in the assessed samples. This mass loss was higher in the 28 day samples, consistent with a lower degree of slag reaction at this time of curing compared with specimens aged for 365 days.

In samples with 10 wt.% limestone (Fig. 8A, 90S1) a higher mass loss below 200 °C was identified after 28 days of curing, compared to samples without limestone. This observation was consistent with the higher total mass loss (Table 4) reported for this cement. The most distinctive feature is the mass loss between 400 °C and 800 °C, associated with decomposition of limestone. In the 28 day sample, two mass losses at 554 °C and 727 °C were observed, corresponding to the decomposition of vaterite and calcite, respectively [89]. At longer curing durations, only decomposition of calcite is identified in these samples. Similarly to the S1 slag cements, small mass losses were identified above 800 °C accompanied by the release of SO_2, consistent with the presence of unreacted slag in the cements.

The percentages of reacted limestone, calculated as indicated in Section 2.2.2 are reported in Table 4. The percentages of limestone which have reacted are broadly comparable between the two slag series, with negligible changes in the amount of limestone reaction beyond 28 days of curing. This indicates that the added limestone remained unreactive at longer curing durations of 180 and 385 days. Thermogravimetric results do not show any increase in calcite content with time, to confirm that no carbonation has occurred during long-term storage and sample preparation. ^{27}Al MAS NMR results (Figs. 5 and 6) indicated

Table 4
Reacted limestone in sulfate-limestone activates slag cements determined by thermogravimetry (estimated uncertainty ± 0.5 %).

Curing time (days)	90S1	90S2
28	3.0 %	3.5 %
180	3.6 %	3.5 %
365	3.6 %	3.7 %

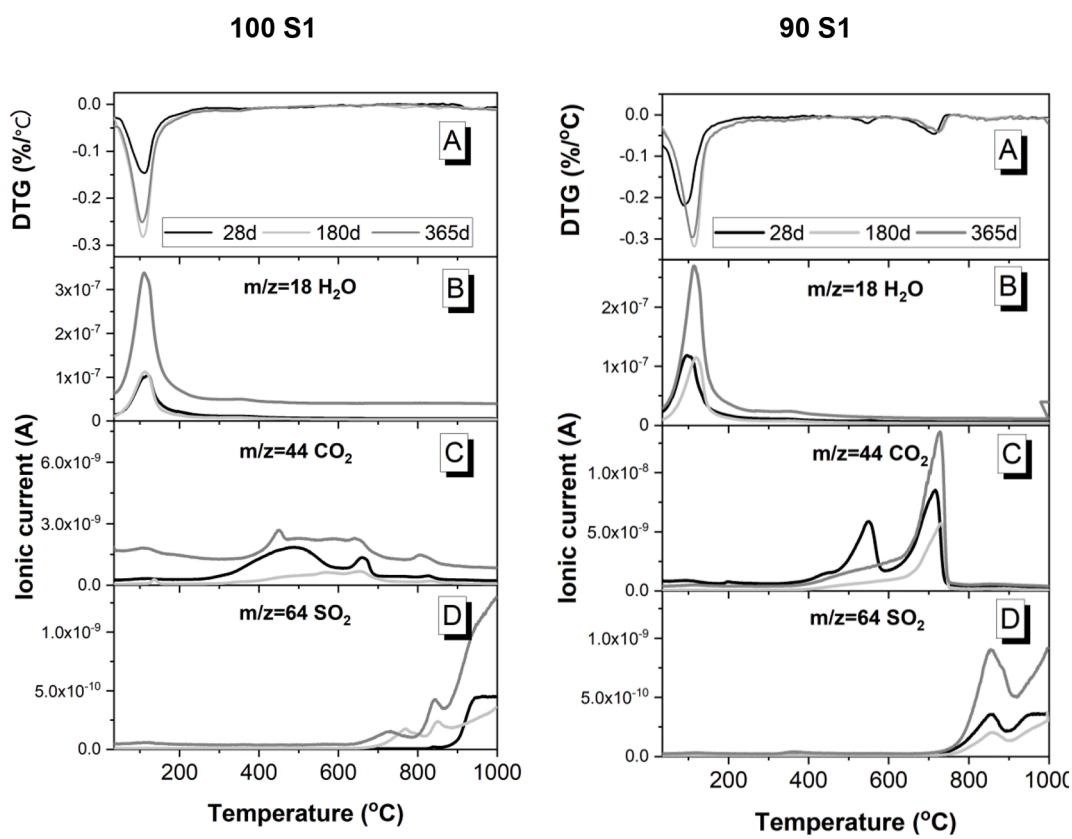

Fig. 8. (A) Differential thermograms (mass loss downwards) sulfate activated slag cements without (100S1) and with (90S1) limestone addition, as a function of curing time. Mass spectra of (B) H_2O, (C) CO_2 and (D) SO_2 are also reported. m/z = mass/charge ratio, for each ion of interest.

the formation of LDHs in these systems. As limestone reaction is very limited in these systems, this supports the earlier suggestion that sulfate-LDH which present an Al resonance at ^{27}Al δ_{iso} = 9 ppm [80] are the most likely LDH phase forming in sodium sulfate activated slag cements.

Derivative curves along with mass spectra for the slag S2 cements are shown in Fig. 9. For samples without limestone addition (Fig. 9A, 100S2) significant differences in the mass loss below 200 °C were observed between 28 and 180 days of curing; however, slight differences were observed between 180 and 365 days of curing. This indicates that a significant amount of hydrated reaction products were forming in this cement at extended curing durations. The addition of limestone to these cements (Fig. 9B, 90S2) induced higher mass losses at 28 days compared to those in samples without limestone (Fig. 9A, 100S2). This difference can be attributed to a higher extent of reaction with the limestone addition. Negligible differences in mass losses were recorded at 180 days of curing (relative to 28 days), with a slight increase in the mass loss after 365 days of curing.

In the S2 slag cement without limestone (Fig. 9A, 100S2), no significant features were observed between 200 °C and 800 °C. A slight mass loss between 800 °C and 1000 °C was consistent with the release of SO_2 from the unreacted slag remaining in these cements. The SO_2 signal was more intense in this temperature for the 28 day cured sample, relative to later curing times. These features are similar to those identified for the S1 slag cement without limestone (Fig. 8A, 100S1).

In the 90S2 paste, comparable mass losses were observed between 600 °C and 800 °C for the different curing durations. This is consistent with the negligible differences in the estimated amount of unreacted limestone (Table 4) between different curing times.

3.3. Compressive strength and pore structure

Fig. 10 presents the compressive strength of 28 days cured sodium sulfate-activated slag pastes. The strength values of the S2 slag based cements were higher than all of the S1 slag based cements, across samples with limestone additions as well as slag-only samples. This is consistent with a slightly higher degree of reaction of slag reaction identified in S2 by thermogravimetry analysis (Fig. 7) at 28 days of curing. These compressive strength values are significantly higher than those reported by Mobasher et al. [30] for sodium sulfate activated slag cements produced with slightly higher activator doses (10 wt.% sodium sulfate), and using slags with different compositions to those studied here. This further highlights the strong dependency between raw materials properties and activation conditions on the properties of sodium

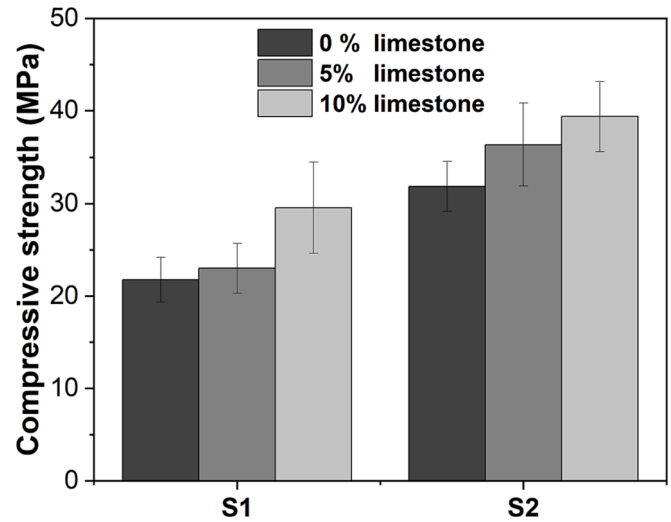

Fig. 10. Compressive strength (at 28 days curing time) of sodium sulfate-activated slag pastes as a function of the slag type and limestone addition. Error bars correspond to one standard deviation of 8 measurements.

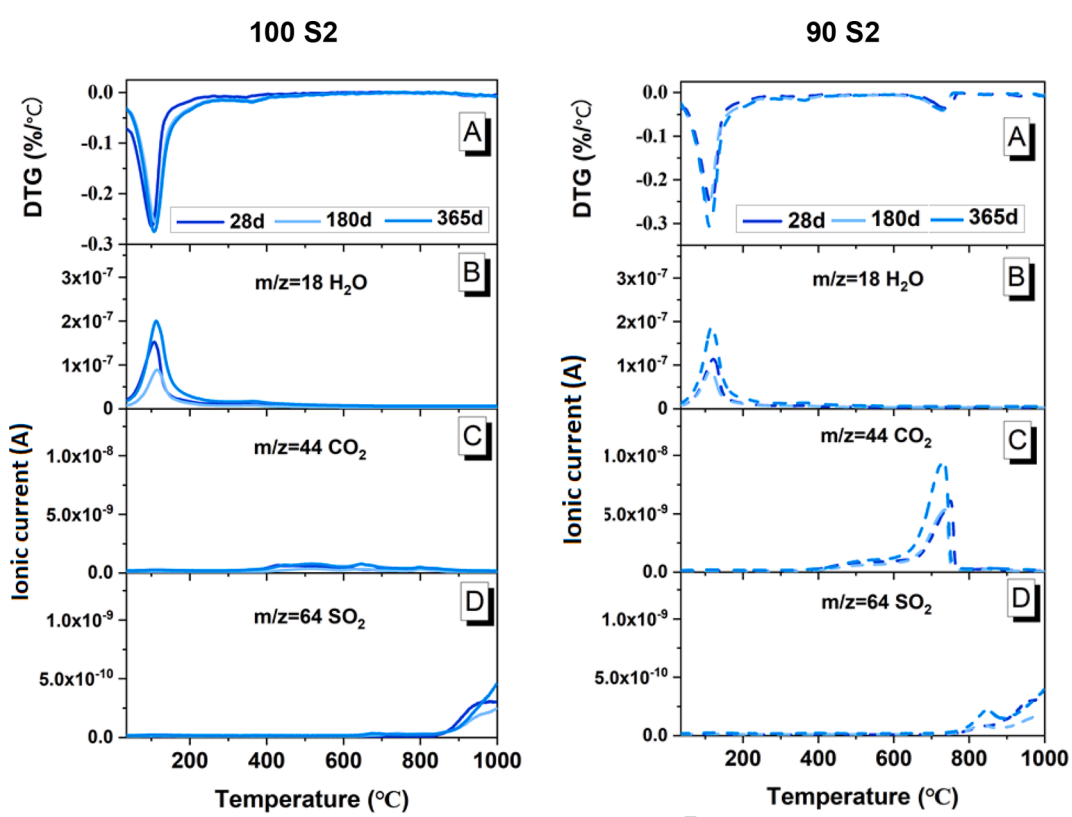

Fig. 9. (A) Differential thermograms (mass loss downwards) sulfate activated slag cements without (100S2) and with (90S2) limestone addition, as a function of curing time. Mass spectra of (B) H_2O, (C) CO_2 and (D) SO_2 are also reported. m/z = mass/charge ratio, for each ion of interest.

sulfate activated slag cements.

The addition of limestone increased the strength in these materials independently of the slag used. This is consistent with the fact that limestone seems to be promoting a faster reaction kinetics in these pastes, as well as formation of LDH type phases at later age. A similar observation was reported by Rashad et al. [93], who identified comparable strengths to those of S2 slag for sodium sulfate activated slag cements with 5 wt.% limestone addition. In that study, a significant increase of the compressive strength in the slag/limestone composite cements was observed at 56 and 90 days of curing, compared to specimens without limestone.

Mercury intrusion porosimetry results are shown in Fig. 11. The sodium sulfate activated slag cements in this study - with or without limestone addition - developed a refined pore structure (i.e. a shift in the cumulative pore volume towards smaller pore entry diameters with narrow range of size distribution) compared to that typically identified in Portland and blended Portland cements [94,95]. Cumulative volumes of mercury intruded increased with the limestone addition (Fig. 11A and 11C), regardless of the slag used. Slag S1-based samples consistently showed higher cumulative intrusion volume compared to slag S2-based samples, independent of limestone addition. The lower cumulative porosity volumes in slag S2-based samples correspond well with the higher compressive strengths for all slag S2-based samples (relative to slag S1-based samples). The lower cumulative volumes suggest that the space filling efficiency (i.e., the reduction of the total pore volume with solid reaction products) is higher for the reaction products formed in slag S2-based samples.

For all samples, the differences in pore volume were mainly in the size range of 10–30 nm, which can be seen in the differential intrusion volume plots (Fig. 11B and 11D). Intrusion pore volumes were higher for pastes containing limestone in these lower pore entry sizes (i.e. 10–30 nm), which are typically attributed to size ranges of gel pores. This observation is consistent with the findings of preceding characteristion techniques – that limestone addition caused an increase in the amount of reaction products. It is thought that the greater quantity of reaction products led to higher amounts of accessible gel pores in these finer pore size ranges, which are thus a proxy measure for increased strength development [48]. The intrusion volume corresponding to the peak size < 30 nm is lower in 100S2 and 90S2 (Fig. 11C and 11D). This indicates that the higher compressive strength developed by S2 slag cements compared with S1 slag cements is at least partly due to the development of a refined pore structure when using lower Al_2O_3 containing slags [48]. Two major aspects can be summarised from these observations on compressive strength and porosity. Firstly, there is lower overall porosity in all slag S2-based systems due to better space filling efficacy of the reaction products from slag S2. Secondly, there is an increase in the gel pore volume in the finer porosity size range due to limestone addition, for cements made with slags S1 or S2. The former mechanism leads to higher strength in all slag S2-based systems and the latter causes improved strength due to limestone addition with both S1 and S2 slag-based systems.

Differences in the critical pore entry size diameter were identified as a function of the slag type and limestone addition (Table 5). The critical pore size corresponds to the highest value in the differential distribution curves, and represents the most frequently occurring pore size within the interconnected pores [48]. Comparable critical pore sizes were identified for sodium sulfate-activated cements solely based on slag, independently of the slag type used. The addition of limestone reduced the critical pore size in S1 slag based cements at replacement levels of 5 wt.% (95S1); however, similar critical pore sizes were observed in samples with 10 wt.% limestone (90 S1) to those in S1 slag-only systems. For the S2 slag based cements, the addition of 5 wt.% limestone (95S2) did not modify the critical pore size; however, a significant increase was identified at higher replacement levels (90 S2).

The overall porosity of sodium sulfate activated slag/limestone composites, determined from MIP, is presented in Table 6. Limestone

Table 5
The critical pore size diameter in nm in sulfate activated slag/limestone composite cements.

Slag ID	Slag content		
	100 wt%	95 wt%	90 wt%
S1	10.6	9.1	10.9
S2	10.5	10.5	13.9

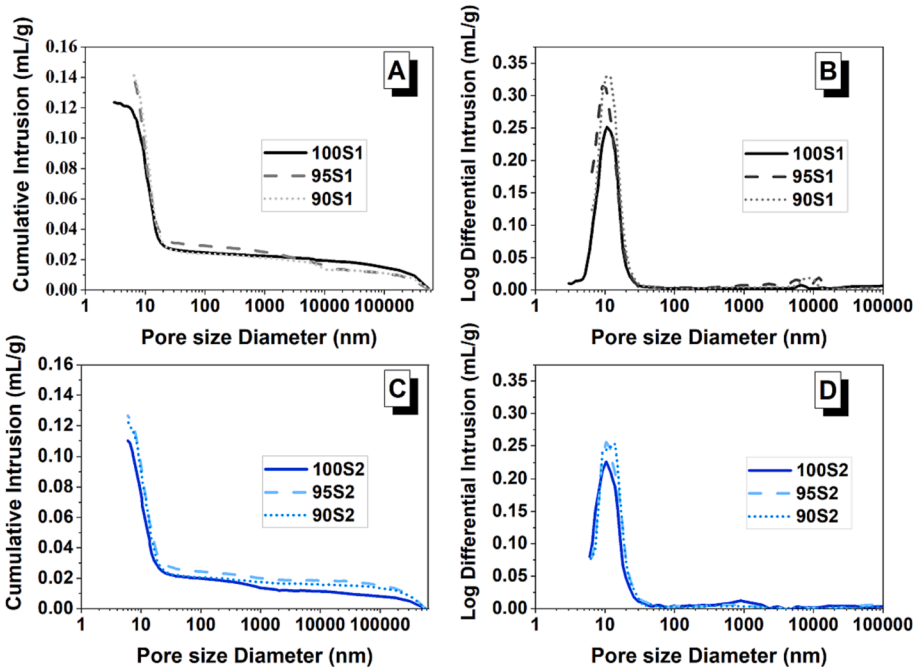

Fig. 11. Pore size distribution of Na_2SO_4-activated slag pastes at 28 days. (A) and (B) show cumulative and differential pore volume for S1 slag pastes. (C) and (D) show cumulative and differential pore volume for S2 slag pastes.

Table 6
Total porosity (in vol.%) of sulfate activated slag/limestone composite cements.

Slag ID	Slag content		
	100 wt%	95 wt%	90 wt%
S1	21.7 %	25.3 %	25.0 %
S2	19.3 %	20.9 %	21.4 %

addition increased the overall porosity, independently of the slag type used. The increase in total porosity due to limestone addition was higher for systems produced with the slag with higher Al_2O_3 content (S1). This was despite the fact the S1 slag exhibited a higher degree of reaction at early ages, as identified by calorimetry (Fig. 1), and extended curing duration, as identified by ^{29}Si MAS NMR analysis (Fig. 4). Composite cements produced with the S2 slag exhibited a lower porosity with or without limestone addition. This is consistent with the higher compressive strength values identified for S2 slag based sulfate activated composite cements (Fig. 10).

In order to quantitatively evaluate the pore structure of sodium sulfate activated slag/limestone composite cements, pores were classified into size categories < 30, 30–100 and > 100 nm [48] as shown on Fig. 12. Slight changes in the fraction of the large capillary pores (>30 nm diameter [96]) were identified with the limestone addition, consistent with the changes observed in the critical pore diameters (Table 5) for these cements. An increased fraction of pore size in the range of 10 to 30 nm, also referred to as medium capillaries [96] was observed upon limestone replacement in these systems. This is attributed to a large portion of limestone remaining as a filler in these cements, as identified by thermogravimetry (Table 4), without contributing to reaction products that could lead to higher capillary pore volume (i.e. the space that needs to be filled by reaction products). Pores with a diameter lower than 10 nm (gel pores) are likely to affect the shrinkage [97]. A higher intruded volume below 10 nm was identified in the S1 slag based cements with 5 wt.% replacement of limestone – this observation is consistent with the reduced critical pore size (Table 5).

4. Conclusions

This study demonstrates that the chemical composition of slag, as well as addition of limestone (5 and 10 wt.%), influences the kinetics of reaction and structural evolution of sodium sulfate-activated slag cements. The slag with a higher Al_2O_3 content was more reactive upon activation with sodium sulfate, albeit it is likely that the nature of the glassy phase itself also has an influence. The addition of limestone accelerates the kinetics of reaction, particularly for the slag with the lower reactivity during the first hours after mixing. However, comparable degrees of reaction are achieved by 14 days of reaction. 28 day compressive strength values are improved with limestone addition.

The main crystalline reaction products forming in these cements were ettringitte and an aluminium substituted calcium silicate hydrate type phase, with a tobermorite type structure, mostly likely a C-(N)-A-S-H type gel. More ettringite seemed to be forming in the cements produced with slags with higher Al_2O_3 content, independent of the amount of limestone added. NMR spectroscopy results revealed that poorly crystalline layered double hydroxide type phases (e.g. AFm or hydrotalcite) are forming in all the cements evaluated, whose prevalence seems to be more noticeable in the cements produced with the slag with lower Al_2O_3.

The slag with lower reactivity upon sodium sulfate activation produced binders with the highest compressive strength after 28 days of curing, independently of the limestone replacement level. This was mainly due to better spacing filling and refined porosity which can be attributed to the differences in the amounts of ettringite/LDHs forming in these systems. Limestone addition increases the finer pore volume < 30 nm, however, there is a positive effect on compressive strength despite higher pore volume < 30 nm.

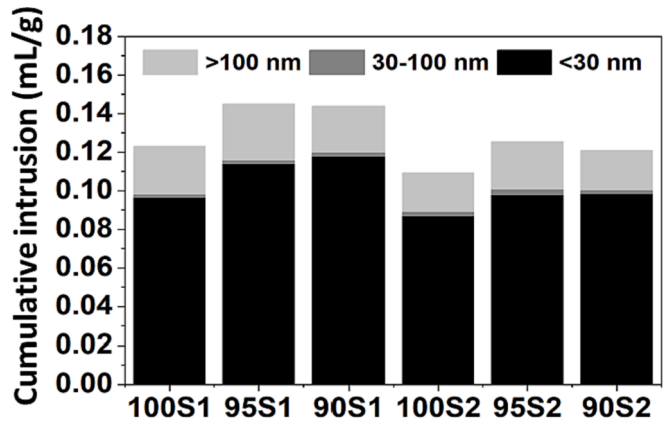

Fig. 12. Pore size fraction in Na_2SO_4-activated pastes using slag S1 and slag S2 with 5 and 10 wt.% limestone substitution.

These findings can help inform the development of both alkali-activated and hybrid alkaline cement systems. The contribution of limestone additions in small quantities is primarily to accelerate kinetics and refine the pore structure. This could have practical benefits for strength development, both at early ages and longer ageing times. Whilst there is some evidence for a small degree of limestone reaction, there is negligible effect on the overall phase assemblage. Whilst the maximum slag replacement trialled in this study is modest (10 wt.%), it nonetheless offers a route to help reduce the demand for slag in the production of sodium sulphate activated slag cements.

Further research is necessary to fully understand the effects of slag chemistry in these systems, particularly around Al_2O_3 content. Whilst the data in this study is unique for its ageing times of up to 365 days, further testing would be valuable for understanding if limestone does play any further role at even longer ageing times. Given the constraints on the global availability of slag, and the relative abundance of limestone, the potential for higher levels of limestone should also be explored.

CRediT authorship contribution statement

Alastair T.M. Marsh: Investigation, Formal analysis, Writing – original draft, Writing – review & editing. **Zengliang Yue:** Formal analysis, Writing – original draft, Writing – review & editing. **Yuvaraj Dhandapani:** Formal analysis, Writing – original draft, Writing – review & editing. **Katharine Button:** Methodology, Investigation, Writing – review & editing. **Samuel Adu-Amankwah:** Conceptualization, Methodology, Formal analysis, Supervision, Writing – review & editing. **Susan A. Bernal:** Conceptualization, Methodology, Formal analysis, Funding acquisition, Supervision, Writing – original draft, Writing – review & editing.

Declaration of Competing Interest

The authors declare that they have no known competing financial interests or personal relationships that could have appeared to influence the work reported in this paper.

Data availability

A DOI link to the data of this article is provided in the paper

Acknowledgements

This study was supported by the School of Civil Engineering at the University of Leeds, and the UK Engineering and Physical Sciences

Research Council (EPSRC) via the Early Career Fellowship EP/R001642/1. The authors are grateful with Vicky Leadley and Leslie Arkless for assistance with NMR measurements, and Dan Geddes from the University of Sheffield for assistance with MIP measurements. The data associated with this paper are openly available from the University of Leeds Data Repository, at https://doi.org/10.5518/1227.

Appendix A. Supplementary data

Supplementary data to this article can be found online at https://doi.org/10.1016/j.conbuildmat.2022.129527.

References

[1] U. Environment, K.L. Scrivener, V.M. John, E.M. Gartner, Eco-efficient cements: Potential economically viable solutions for a low-CO_2 cement-based materials industry, Cem. Concr. Res. 114 (2018) 2–26.
[2] M.C.G. Juenger, R. Siddique, Recent advances in understanding the role of supplementary cementitious materials in concrete, Cem. Concr. Res. 78 (2015) 71–80.
[3] I. Jawed, J. Skalny, Alkalies in cement: a review: II. Effects of alkalies on hydration and performance of Portland cement, Cem. Concr. Res. 8 (1) (1978) 37–51.
[4] C. Shi, A. Fernández-Jiménez, A. Palomo, New cements for the 21st century: The pursuit of an alternative to Portland cement, Cem. Concr. Res. 41 (7) (2011) 750–763.
[5] L. Xue, Z. Zhang, H. Wang, Early hydration kinetics and microstructure development of hybrid alkali activated cements (HAACs) at room temperature, Cem. Concr. Compos. 123 (2021) 104200.
[6] J.M. Mejía, E. Rodríguez, R. Mejía de Gutiérrez, N. Gallego, Preparation and characterization of a hybrid alkaline binder based on a fly ash with no commercial value, J. Cleaner Prod. 104 (2015) 346–352.
[7] A. Palomo, A. Fernández-Jiménez, G. Kovalchuk, L.M. Ordoñez, M.C. Naranjo, OPC-fly ash cementitious systems: study of gel binders produced during alkaline hydration, J. Mater. Sci. 42 (9) (2007) 2958–2966.
[8] I. García-Lodeiro, A. Fernández-Jiménez, A. Palomo, Variation in hybrid cements over time. Alkaline activation of fly ash–portland cement blends, Cem. Concr. Res. 52 (2013) 112–122.
[9] L. Xue, Z. Zhang, H. Wang, Hydration mechanisms and durability of hybrid alkaline cements (HACs): A review, Constr. Build. Mater. 266 (2021) 121039.
[10] S. Park, K.A. Moges, S. Wu, S. Pyo, Characteristics of hybrid alkaline cement composites with high cement content: flash set and high compressive strength, J. Mater. Res. Technol. 17 (2022) 1582–1597.
[11] Á. Palomo, E. Kavalerova, A. Fernández-Jiménez, P. Krivenko, I. García-Lodeiro, O. Maltseva, A review on alkaline activation: new analytical perspectives, Materiales de Construccion 64 (315) (2014).
[12] D.F. Velandia, C.J. Lynsdale, J.L. Provis, F. Ramirez, A. Gomez, Evaluation of activated high volume fly ash systems using Na_2SO_4, lime and quicklime in mortars with high loss on ignition fly ashes, Constr. Build. Mater. 128 (2016) 248–255.
[13] D.F. Velandia, C.J. Lynsdale, J.L. Provis, F. Ramirez, Effect of mix design inputs, curing and compressive strength on the durability of Na_2SO_4-activated high volume fly ash concretes, Cem. Concr. Compos. 91 (2018) 11–20.
[14] F. Zou, C. Hu, F. Wang, Y. Ruan, S. Hu, Enhancement of early-age strength of the high content fly ash blended cement paste by sodium sulfate and C-S–H seeds towards a greener binder, J. Cleaner Prod. 244 (2020) 118566.
[15] S. Joseph, R. Snellings, Ö. Cizer, Activation of Portland cement blended with high volume of fly ash using Na_2SO_4, Cem. Concr. Compos. 104 (2019) 103417.
[16] J. Fu, M.W. Bligh, I. Shikhov, A.M. Jones, C. Holt, L.M. Keyte, F. Moghaddam, C. H. Arns, S.J. Foster, T.D. Waite, A microstructural investigation of a Na_2SO_4 activated cement-slag blend, Cem. Concr. Res. 150 (2021) 106609.
[17] J. Fu, A.M. Jones, M.W. Bligh, C. Holt, L.M. Keyte, F. Moghaddam, S.J. Foster, T. D. Waite, Mechanisms of enhancement in early hydration by sodium sulfate in a slag-cement blend – Insights from pore solution chemistry, Cem. Concr. Res. 135 (2020) 106110.
[18] G. Li, P. Le Bescop, M. Moranville-Regourd, Synthesis of the U phase ($4CaO.0.9Al_2O_3$ $1.1SO_3.0.5Na_2O.16H_2O$), Cem. Concr. Res. 27 (1) (1997) 7–13.
[19] G. Li, P. Le Bescop, M. Moranville, The U phase formation in cement-based systems containing high amounts of Na_2SO_4, Cem. Concr. Res. 26 (1) (1996) 27–33.
[20] J.L. Provis, S.A. Bernal, Binder chemistry–blended systems and intermediate Ca content, in: J.L. Provis, J.S. van Deventer (Eds.), Alkali Activated Materials, Springer2014, pp. 125-144.
[21] G. Li, P. Le Bescop, M. Moranville, Expansion mechanism associated with the secondary formation of the U phase in cement-based systems containing high amounts of Na_2SO_4, Cem. Concr. Res. 26 (2) (1996) 195–201.
[22] Y. Elakneswaran, C. Li, T. Kajio, E. Owaki, M. Ogino, T. Nawa, Durability of slag-blended cement due to U-phase instability in sulphate environment, Mater. Struct. 53 (6) (2020) 146.
[23] G. Sant, A. Kumar, C. Patapy, G. Le Saout, K. Scrivener, The influence of sodium and potassium hydroxide on volume changes in cementitious materials, Cem. Concr. Res. 42 (11) (2012) 1447–1455.
[24] B. Mota, T. Matschei, K. Scrivener, Impact of NaOH and Na_2SO_4 on the kinetics and microstructural development of white cement hydration, Cem. Concr. Res. 108 (2018) 172–185.
[25] A. Adesina, C. Rodrigue Kaze, Physico-mechanical and microstructural properties of sodium sulfate activated materials: A review, Constr. Build. Mater. 295 (2021), 123668.
[26] S.A. Bernal, Advances in near-neutral salts activation of blast furnace slags, RILEM Tech. Lett. 1 (2016) 39-39.
[27] A.M. Rashad, Y. Bai, P.A.M. Basheer, N.C. Collier, N.B. Milestone, Chemical and mechanical stability of sodium sulfate activated slag after exposure to elevated temperature, Cem. Concr. Res. 42 (2) (2012) 333–343.
[28] N. Mobasher, S.A. Bernal, O.H. Hussain, D.C. Apperley, H. Kinoshita, J.L. Provis, Characterisation of $Ba(OH)_2$–Na_2SO_4–blast furnace slag cement-like composites for the immobilisation of sulfate bearing nuclear wastes, Cem. Concr. Res. 66 (2014) 64–74.
[29] A.M. Rashad, Y. Bai, P.A.M. Basheer, N.B. Milestone, N.C. Collier, Hydration and properties of sodium sulfate activated slag, Cem. Concr. Compos. 37 (2013) 20–29.
[30] N. Mobasher, S.A. Bernal, J.L. Provis, Structural evolution of an alkali sulfate activated slag cement, J. Nucl. Mater. 468 (2016) 97–104.
[31] M. Ben Haha, B. Lothenbach, G. Le Saout, F. Winnefeld, Influence of slag chemistry on the hydration of alkali-activated blast-furnace slag—Part I: Effect of MgO, Cem. Concr. Res. 41 (9) (2011) 955–963.
[32] S.A. Bernal, R. San Nicolas, R.J. Myers, R.M. de Gutiérrez, F. Puertas, J.S. van Deventer, J.L. Provis, MgO content of slag controls phase evolution and structural changes induced by accelerated carbonation in alkali-activated binders, Cem. Concr. Res. 57 (2014) 33–43.
[33] K.D. Ingram, K.E. Daugherty, A review of limestone additions to Portland cement and concrete, Cem. Concr. Compos. 13 (3) (1991) 165–170.
[34] B. Lothenbach, G. Le Saout, E. Gallucci, K. Scrivener, Influence of limestone on the hydration of Portland cements, Cem. Concr. Res. 38 (6) (2008) 848–860.
[35] S. Adu-Amankwah, M. Zajac, C. Stabler, B. Lothenbach, L. Black, Influence of limestone on the hydration of ternary slag cements, Cem. Concr. Res. 100 (2017) 96–109.
[36] M. Sharma, S. Bishnoi, F. Martirena, K. Scrivener, Limestone calcined clay cement and concrete: A state-of-the-art review, Cem. Concr. Res. 149 (2021) 106564.
[37] Y. Dhandapani, M. Santhanam, G. Kaladharan, S. Ramanathan, Towards ternary binders involving limestone additions—A review, Cem. Concr. Res. 143 (2021) 106396.
[38] G. Millán-Corrales, J. González-López, A. Palomo, A. Fernandez-Jiménez, Replacing fly ash with limestone dust in hybrid cements, Constr. Build. Mater. 243 (2020) 118169.
[39] M. Wu, Y. Zhang, Y. Jia, W. She, G. Liu, Y. Yang, Z. Rong, W. Sun, The influence of chemical admixtures on the strength and hydration behavior of lime-based composite cementitious materials, Cem. Concr. Compos. 103 (2019) 353–364.
[40] R. Khoshnazar, J. Beaudoin, L. Raki, R. Alizadeh, Solvent exchange in sulphoaluminate phases. Part I: ettringite, Adv. Cem. Res. 25 (6) (2013) 314–321.
[41] Z. Zhang, G.W. Scherer, Physical and chemical effects of isopropanol exchange in cement-based materials, Cem. Concr. Res. 145 (2021) 106461.
[42] P. Giraudeau, I. Tea, G.S. Remaud, S. Akoka, Reference and normalization methods: Essential tools for the intercomparison of NMR spectra, J. Pharm. Biomed. Anal. 93 (2014) 3–16.
[43] E. Berodier, K. Scrivener, Understanding the Filler Effect on the Nucleation and Growth of C-S-H, J. Am. Ceram. Soc. 97 (12) (2014) 3764–3773.
[44] T. Oey, A. Kumar, J.W. Bullard, N. Neithalath, G. Sant, The filler effect: the influence of filler content and surface area on cementitious reaction rates, J. Am. Ceram. Soc. 96 (6) (2013) 1978–1990.
[45] M. Ben Haha, B. Lothenbach, G. Le Saout, F. Winnefeld, Influence of slag chemistry on the hydration of alkali-activated blast-furnace slag—Part II: Effect of Al_2O_3, Cem. Concr. Res. 42 (1) (2012) 74–83.
[46] A. Gruskovnjak, B. Lothenbach, F. Winnefeld, R. Figi, S.-C. Ko, M. Adler, U. Mäder, Hydration mechanisms of super sulphated slag cement, Cem. Concr. Res. 38 (7) (2008) 983–992.
[47] S. Blotevogel, A. Ehrenberg, L. Steger, L. Doussang, J. Kaknics, C. Patapy, M. Cyr, Ability of the R3 test to evaluate differences in early age reactivity of 16 industrial ground granulated blast furnace slags (GGBS), Cem. Concr. Res. 130 (2020) 105998.
[48] M. Zajac, J. Skocek, S. Adu-Amankwah, L. Black, M. Ben Haha, Impact of microstructure on the performance of composite cements: Why higher total porosity can result in higher strength, Cem. Concr. Compos. 90 (2018) 178–192.
[49] J. Skibsted, C. Hall, Characterization of cement minerals, cements and their reaction products at the atomic and nano scale, Cem. Concr. Res. 38 (2) (2008) 205–225.
[50] G. Puerta-Falla, M. Balonis, G. Le Saout, A. Kumar, M. Rivera, G. Falzone, N. Neithalath, G. Sant, The influence of slightly and highly soluble carbonate salts on phase relations in hydrated calcium aluminate cements, J. Mater. Sci. 51 (12) (2016) 6062–6074.
[51] S. Krishnan, A.C. Emmanuel, S. Bishnoi, Hydration and phase assemblage of ternary cements with calcined clay and limestone, Constr. Build. Mater. 222 (2019) 64–72.
[52] B. Lothenbach, D.A. Kulik, T. Matschei, M. Balonis, L. Baquerizo, B. Dilnesa, G. D. Miron, R.J. Myers, Cemdata18: A chemical thermodynamic database for hydrated Portland cements and alkali-activated materials, Cem. Concr. Res. 115 (2019) 472–506.
[53] C. Baerlocher, L.B. McCusker, D.H. Olson, Atlas of Zeolite Framework Types, Elsevier, 2007.
[54] S.A. Bernal, J.L. Provis, V. Rose, R. Mejía de Gutierrez, Evolution of binder structure in sodium silicate-activated slag-metakaolin blends, Cem. Concr. Compos. 33 (1) (2011) 46–54.

[55] S.A. Bernal, R. Mejía de Gutierrez, J.L. Provis, V. Rose, Effect of silicate modulus and metakaolin incorporation on the carbonation of alkali silicate-activated slags, Cem. Concr. Res. 40 (6) (2010) 898–907.
[56] S.A. Bernal, Microstructural changes induced by CO_2 Exposure in alkali-activated slag/metakaolin pastes, Front. Mater. 3 (2016).
[57] R.J. Myers, S.A. Bernal, J.L. Provis, Phase diagrams for alkali-activated slag binders, Cem. Concr. Res. 95 (2017) 30–38.
[58] M. Maldonado, M.D. Oleksiak, S. Chinta, J.D. Rimer, Controlling crystal polymorphism in organic-free synthesis of Na-zeolites, J. Am. Chem. Soc. 135 (7) (2013) 2641–2652.
[59] A. Navrotsky, O. Trofymluk, A.A. Levchenko, Thermochemistry of microporous and mesoporous materials, Chem. Rev. 109 (9) (2009) 3885–3902.
[60] M.D. Jackson, J. Moon, E. Gotti, R. Taylor, S.R. Chae, M. Kunz, A.-H. Emwas, C. Meral, P. Guttmann, P. Levitz, H.-R. Wenk, P.J.M. Monteiro, Material and elastic properties of Al-Tobermorite in ancient roman seawater concrete, J. Am. Ceram. Soc. 96 (8) (2013) 2598–2606.
[61] G. Engelhardt, D. Michel, High-resolution solid-state NMR of silicates and zeolites, (1987).
[62] P.J. Schilling, L.G. Butler, A. Roy, H. Eaton, ^{29}Si and ^{27}Al MAS-NMR of NaOH-activated blast-furnace slag, J. Am. Ceram. Soc. 77 (9) (1994) 2363–2368.
[63] R.J. Myers, S.A. Bernal, R. San Nicolas, J.L. Provis, Generalized structural description of calcium–sodium aluminosilicate hydrate gels: the cross-linked substituted tobermorite model, Langmuir 29 (17) (2013) 5294–5306.
[64] R. Snellings, Surface chemistry of calcium aluminosilicate glasses, J. Am. Ceram. Soc. 98 (1) (2015) 303–314.
[65] R.J. Myers, S.A. Bernal, J.D. Gehman, J.S.J. van Deventer, J.L. Provis, The role of Al in cross-linking of alkali-activated slag cements, J. Am. Ceram. Soc. 98 (3) (2015) 996–1004.
[66] R.J. Myers, J.L. Provis, B. Lothenbach, Composition–solubility–structure relationships in calcium (alkali) aluminosilicate hydrate (C-(N, K-) ASH), Dalton Trans. 44 (30) (2015) 13530–13544.
[67] B. Walkley, S.J. Page, G.J. Rees, J.L. Provis, J.V. Hanna, Nanostructure of CaO-(Na_2O)-Al_2O_3-SiO_2-H_2O gels revealed by multinuclear solid-state magic angle spinning and multiple quantum magic angle spinning nuclear magnetic resonance spectroscopy, J. Phys. Chem. C 124 (2) (2019) 1681–1694.
[68] B. Walkley, X. Ke, J.L. Provis, S.A. Bernal, Activator anion Influences the nanostructure of alkali-activated slag cements, J. Phys. Chem. C 125 (37) (2021) 20727–20739.
[69] B. Lothenbach, E. Bernard, U. Mäder, Zeolite formation in the presence of cement hydrates and albite, Phys. Chem. Earth, Parts A/B/C 99 (2017) 77–94.
[70] G. Engelhardt, Multinuclear solid-state NMR in silicate and zeolite chemistry, TrAC, Trends Anal. Chem. 8 (9) (1989) 343–347.
[71] R.K. Harris, A. Samadi-Maybodi, W. Smith, The incorporation of aluminum into silicate ions in alkaline aqueous solutions, studied by aluminum-27 NMR, Zeolites 19 (2–3) (1997) 147–155.
[72] A. Navrotsky, Physics and Chemistry of Earth Materials, Cambridge University Press, 1994.
[73] A.K. Varshneya, Fundamentals of Inorganic Glasses, Elsevier, 2013.
[74] S. Kucharczyk, M. Zajac, C. Stabler, R.M. Thomsen, M.B. Haha, J. Skibsted, J. Deja, Structure and reactivity of synthetic CaO-Al2O3-SiO2 glasses, Cem. Concr. Res. 120 (2019) 77–91.
[75] K.J. MacKenzie, M.E. Smith, Multinuclear Solid-state Nuclear Magnetic Resonance of Inorganic Materials, Elsevier, 2002.
[76] P. Wang, R. Trettin, V. Rudert, T. Spaniol, Influence of Al2O3 content on hydraulic reactivity of granulated blast-furnace slag, and the interaction between Al2O3 and CaO, Adv. Cem. Res. 16 (1) (2004) 1–7.
[77] B. Walkley, J.L. Provis, Solid-state nuclear magnetic resonance spectroscopy of cements, Mater. Today Adv. 1 (2019) 100007.
[78] J. Skibsted, E. Henderson, H. Jakobsen, Characterization of calcium aluminate phases in cements by aluminum-27 MAS NMR spectroscopy, Inorg. Chem. 32 (6) (1993) 1013–1027.
[79] F. Rey, V. Fornés, J.M. Rojo, Thermal decomposition of hydrotalcites. An infrared and nuclear magnetic resonance spectroscopic study, J. Chem. Soc., Faraday Trans. 88 (15) (1992) 2233–2238.
[80] E. Bernard, W.J. Zucha, B. Lothenbach, U. Mäder, Stability of hydrotalcite (Mg-Al layered double hydroxide) in presence of different anions, Cem. Concr. Res. 152 (2022) 106674.
[81] J.L. Provis, S.A. Bernal, Geopolymers and related alkali-activated materials, Annu. Rev. Mater. Res. 44 (2014) 299–327.
[82] M.D. Andersen, H.J. Jakobsen, J. Skibsted, Incorporation of aluminum in the calcium silicate hydrate (C−S-H) of hydrated Portland cements: A high-field ^{27}Al and ^{29}Si MAS NMR investigation, Inorg. Chem. 42 (7) (2003) 2280–2287.
[83] M.A. Kunhi, P. Moutzouri, P. Berruyer, B.J. Walder, J. Siramanont, M. Harris, M. Negroni, S.C. Galmarini, S.C. Parker, K.L. Scrivener, L. Emsley, P. Bowen, The atomic-level structure of cementitious calcium aluminate silicate hydrate, J. Am. Chem. Soc. 142 (25) (2020) 11060–11071.
[84] R.J. Kirkpatrick, K.A. Smith, S. Schramm, G. Turner, W.-H. Yang, Solid-state nuclear magnetic resonance spectroscopy of minerals, Annu. Rev. Earth Planet. Sci. 13 (1) (1985) 29–47.
[85] J. Klinowski, Recent advances in solid-state NMR of zeolites, Annu. Rev. Mater. Sci. 18 (1) (1988) 189–218.
[86] P. Moutzouri, L. Emsley, The atomic-level structure of cementitious calcium aluminate silicate hydrate determined by NMR, Chimia 74 (4) (2021) 272.
[87] E. L'Hôpital, B. Lothenbach, K. Scrivener, D.A. Kulik, Alkali uptake in calcium alumina silicate hydrate (C-A-S-H), Cem. Concr. Res. 85 (2016) 122–136.
[88] C. Hall, P. Barnes, A.D. Billimore, A.C. Jupe, X. Turrillas, Thermal decomposition of ettringite $Ca_6[Al(OH)_6]_2(SO_4)_3{\cdot}26H_2O$, Faraday Trans. 92 (12) (1996) 2125–2129.
[89] M. Maciejewski, H.-R. Oswald, A. Reller, Thermal transformations of vaterite and calcite, Thermochim. Acta 234 (1994) 315–328.
[90] D.P. Prentice, L. Gomez-Zamorano, M. Balonis, B. Erdemli, K. Ellison, N. Neithalath, D. Simonetti, G. Sant, The effects of (di-, tri-valent)-cation partitioning and intercalant anion-type on the solubility of hydrotalcites, J. Am. Ceram. Soc. 103 (10) (2020) 6025–6039.
[91] S.A. Bernal, X. Ke, O. Hussein, J.L. Provis, Effect of testing condition on the loss on ignition results of anhydrous granulated blast furnace slags determined via thermogravimetry, Segment on Concrete with Supplementary Cementitious Materials, RILEM Publications SARL, 2016, pp. 299-299.
[92] S.A. Bernal, M.C. Juenger, X. Ke, W. Matthes, B. Lothenbach, N. De Belie, J. L. Provis, Characterization of supplementary cementitious materials by thermal analysis, Mater. Struct. 50 (1) (2017) 1–13.
[93] A.M. Rashad, Influence of different additives on the properties of sodium sulfate activated slag, Constr. Build. Mater. 79 (2015) 379–389.
[94] Z. Yu, G. Ye, The pore structure of cement paste blended with fly ash, Constr. Build. Mater. 45 (2013) 30–35.
[95] Y. Dhandapani, M. Santhanam, Assessment of pore structure evolution in the limestone calcined clay cementitious system and its implications for performance, Cem. Concr. Compos. 84 (2017) 36–47.
[96] K. Aligizaki, Pore structure of cement-based materials, in: A. Bentur, S. Mindess (Eds.), Modern Concrete Technology Series, Taylor & Francis Group, New York, 2006.
[97] P. Pipilikaki, M. Beazi-Katsioti, The assessment of porosity and pore size distribution of limestone Portland cement pastes, Constr. Build. Mater. 23 (5) (2009) 1966–1970.